

# Protein-Induced Membrane Curvature Investigated through Molecular Dynamics Flexible Fitting

Jen Hsin,<sup>†‡</sup> James Gumbart,<sup>†‡</sup> Leonardo G. Trabuco,<sup>‡§</sup> Elizabeth Villa,<sup>‡§</sup> Pu Qian,<sup>¶</sup> C. Neil Hunter,<sup>¶</sup> and Klaus Schulten<sup>†‡\*</sup>

<sup>†</sup>Department of Physics, <sup>‡</sup>Beckman Institute for Advanced Science and Technology, <sup>§</sup>Center for Biophysics and Computational Biology, University of Illinois at Urbana-Champaign, Urbana, Illinois; and <sup>¶</sup>Department of Molecular Biology and Biotechnology, University of Sheffield, Sheffield, United Kingdom

**ABSTRACT** In the photosynthetic purple bacterium *Rhodobacter (Rba.) sphaeroides*, light is absorbed by membrane-bound light-harvesting (LH) proteins LH1 and LH2. LH1 directly surrounds the reaction center (RC) and, together with PufX, forms a dimeric (RC-LH1-PufX)<sub>2</sub> protein complex. In LH2-deficient *Rba. sphaeroides* mutants, RC-LH1-PufX dimers aggregate into tubular vesicles with a radius of ~250–550 Å, making RC-LH1-PufX one of the few integral membrane proteins known to actively induce membrane curvature. Recently, a three-dimensional electron microscopy density map showed that the *Rba. sphaeroides* RC-LH1-PufX dimer exhibits a prominent bend at its dimerizing interface. To investigate the curvature properties of this highly bent protein, we employed molecular dynamics simulations to fit an all-atom structural model of the RC-LH1-PufX dimer within the electron microscopy density map. The simulations reveal how the dimer produces a membrane with high local curvature, even though the location of PufX cannot yet be determined uniquely. The resulting membrane curvature agrees well with the size of RC-LH1-PufX tubular vesicles, and demonstrates how the local curvature properties of the RC-LH1-PufX dimer propagate to form the observed long-range organization of the *Rba. sphaeroides* tubular vesicles.

## INTRODUCTION

Geometrical curvature is ubiquitous in biological membranes and is essential for key cellular processes, such as endocytosis, cellular fusion, and cellular compartmentalization. Several possible mechanisms shaping the cellular membrane have been proposed, one of which involves integral membrane proteins that induce membrane curvature either through geometrical shape or aggregation properties (1–5). Recently, molecular dynamics (MD) studies of the *Rhodobacter (Rba.) sphaeroides* light-harvesting complex I (LH1) and light-harvesting complex II (LH2) showed that both proteins induce membrane curvature, revealing how these proteins build the spherical membrane vesicles, the photosynthetic chromatophores, that house these proteins (6).

The mechanisms by which LH1 and LH2 shape the photosynthetic membrane were found to differ from each other (6). LH1, in complex with the reaction center (RC) and an additional polypeptide at an undetermined location (7–14), PufX, forms an S-shaped (RC-LH1-PufX)<sub>2</sub> dimeric complex that measures ~200 Å along the long dimer axis and 100 Å along the short dimer axis (Fig. 1). A modeled RC-LH1-PufX dimer placed in a membrane developed a bend at its dimerizing interface in an all-atom simulation within 20 ns, forcing the surrounding membrane to adapt to the dimer's shape and

become curved (6). The RC-LH1-PufX dimer, hence, bends the membrane through its intrinsic geometric shape (6,15).

LH2 curves the membrane by a different mechanism. In all-atom simulations, seven ring-shaped LH2 complexes in an array were observed to pack and tilt away from their neighbors on the cytoplasmic side, creating an overall curved protein aggregate, which pulls the surrounding membrane along, thereby curving it (6). Hence, the membrane-curving properties of the LH2 complex depend upon its aggregation properties.

LH1 and LH2 also differ in another aspect in regard to their curvature properties: although LH2s induce isotropic curvature and form spherical vesicles, RC-LH1-PufX dimers induce anisotropic curvature and form cylindrical tubes as seen in *Rba. sphaeroides* mutants lacking LH2 (8,15–19). This difference in directionality was also observed in the MD studies (6), demonstrating that realistic membrane shaping in atomic detail is feasible using MD.

Indeed, the membrane curvature induced by LH2 in Chandler et al. (6) roughly agreed with the known radius of the photosynthetic vesicles (20). However, in the case of the RC-LH1-PufX dimer, the bending seen in the simulations was less than what was measured in tubular vesicles (8,15–18), i.e., a full explanation of RC-LH1-PufX-induced membrane curvature seemed to be lacking. Recent electron microscopy (EM) single-particle analysis of the negatively stained *Rba. sphaeroides* RC-LH1-PufX dimer at 25 Å resolution showed, though, that the RC-LH1-PufX dimer is more prominently bent than seen in the simulations (6), with a bending angle of ~146° (15), rather than the ~172° seen in silico (180° corresponds to no bending). It is likely that

Submitted February 8, 2009, and accepted for publication April 7, 2009.

\*Correspondence: kschulte@ks.uiuc.edu

Elizabeth Villa's present address is Department of Structural Molecular Biology, Max Planck Institute for Biochemistry, 82152 Martinsried, Germany.

Editor: Nathan Andrew Baker.

© 2009 by the Biophysical Society  
0006-3495/09/07/0321/9 \$2.00

doi: 10.1016/j.bpj.2009.04.031

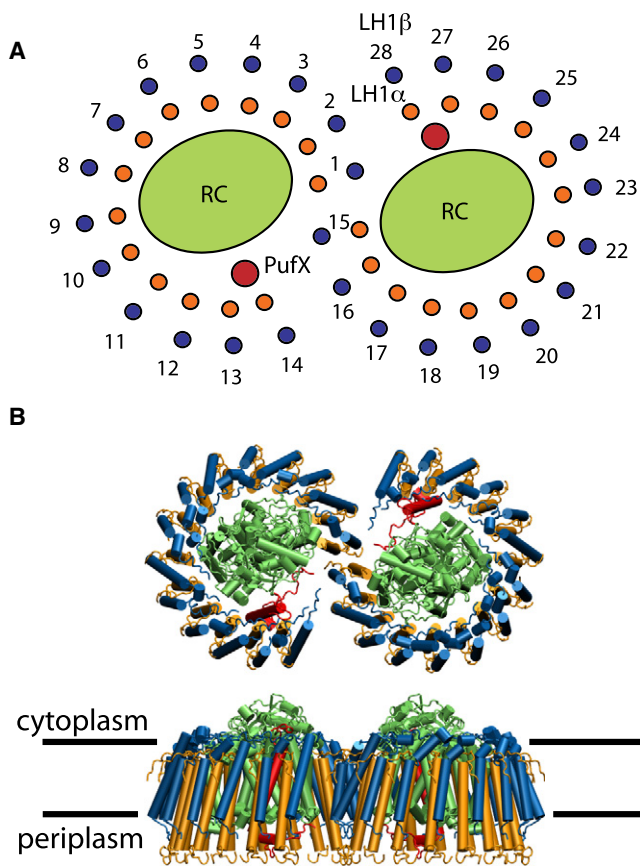


**FIGURE 1** Organization of the *Rba. sphaeroides* RC-LH1-PufX dimer. (A) Schematic of the RC-LH1-PufX dimer organization suggested by the two-dimensional cryo-EM projection study (10). The RC is colored in green, LH1 $\alpha$  in orange, LH1 $\beta$  in blue, and PufX in red. (B) Top and side views of the all-atom model for the *Rba. sphaeroides* RC-LH1-PufX dimer constructed in Chandler et al. (6). The approximate position of the lipid bilayer is indicated. The coloring scheme of the proteins is the same as in panel A.

the simulations performed in Chandler et al. (6), which started from an initially flat RC-LH1-PufX model (Fig. 1 B), require longer time than the simulated 20 ns for the dimer to undergo the large-scale reorganization needed to reach the full bending seen in the EM experiment. Unfortunately, simulations of an RC-LH1-PufX dimer embedded in a membrane consist of 700,000–900,000 atoms, and cannot be extended much further in time than achieved in Chandler et al. (6). We therefore sought to combine the structural information provided in the EM map with the all-atom model developed in Chandler et al. (6), employing for this purpose the methodology described in Trabuco et al. (21). This methodology, termed molecular dynamics flexible fitting (MDFF), accelerates dimer bending, and thereby permits one to observe the effect of the bent dimer on membrane geometry.

The MDFF method (21) has already been successfully applied in Villa et al. (22) to fit a crystallographic structure of the ribosome into an EM map of a ribosome functional state. Here we use MDFF to fit the all-atom model of RC-LH1-PufX dimer constructed in Chandler et al. (6) into the

EM map reported in Qian et al. (15). Two issues can be addressed in obtaining an atomic model of the bent RC-LH1-PufX dimer through MDFF: first, the RC-LH1-PufX dimer contains light-absorbing bacteriochlorophylls, and the spatial arrangement of the bacteriochlorophyll array dictates its excitonic properties; second, the bent geometry of the RC-LH1-PufX dimer can induce high local curvature in the membrane. We have discussed the first issue in Şener et al. (23); here we report on how the RC-LH1-PufX dimer shape the photosynthetic membrane and, thereby, explain the long-range organization of the tubular vesicles seen in LH2-deficient mutants of *Rba. sphaeroides*. As it appears that the curvature properties seen depend mainly on the geometrical shape of the dimer and the interaction between lipids and the LH1 transmembrane helices at the edge of the dimer, we expect that the results reported hold irrespective of an altered PufX location (7).

## METHODS

### The all-atom model of RC-LH1-PufX

Currently, there is no high-resolution structure available for the complete *Rba. sphaeroides* RC-LH1-PufX dimer. An all-atom *Rba. sphaeroides* RC-LH1-PufX dimer model was hence built on the basis of available experimental data as reported in Chandler et al. (6); here we summarize its construction. Structurally, each LH1 dimer consists of 28 pairs of transmembrane helices arranged in the shape of two connected open rings, each enclosing an RC (Fig. 1 A). The inner helices are termed  $\alpha$ -apoproteins and the outer helices  $\beta$ -apoproteins. In between each pair of  $\alpha/\beta$ -apoproteins are located the light-absorbing pigment molecules: two bacteriochlorophylls and one carotenoid. The location of PufX within the complex is still under debate (7–13). The highest resolution two-dimensional cryo-EM density map suggested that PufX is located near the openings of the LH1 rings (10).

For the LH1  $\beta$ -apoprotein, we used the nuclear magnetic resonance solution structure (PDB entry 1DX7) (24). Lacking an LH1  $\alpha$ -apoprotein structure for *Rba. sphaeroides*, we used the solution structure of *Rhodospirillum (Rsp.) rubrum* LH1 $\alpha$  (PDB entry 1XRD) (25) for homology modeling. The pigments were placed in between the  $\alpha/\beta$ -apoprotein pair to form an LH1 subunit (26). The resulting LH1 subunit model was replicated into 28 copies and arranged into the S-shaped dimer as observed in the two-dimensional cryo-EM projection data (10). Two RCs (PDB entry 1PCR) (27) and two PufX proteins (PDB entry 2NRG) (28) were then placed inside the LH1-RC dimer at the locations suggested in Qian et al. (10). The constructed all-atom model of the RC-LH1-PufX dimer is shown in Fig. 1 B.

### Simulation systems

As pointed out already, the results of simulations performed in this study were also used in a separate study of bacteriochlorophyll organization in RC-LH1-PufX (23). The complete RC-LH1-PufX model was placed in a 320 Å × 170 Å membrane patch composed of 50% POPE and 50% POPG lipids, with the two lipid types randomly distributed in both sides of the bilayer (Fig. S1). In simulation Sim1 (see Table 1), the protein/lipid system was placed in a water box of size 350 Å × 200 Å × 120 Å, the size being chosen larger than the lipid patch such that the membrane is effectively independent from its periodic neighbors. The choice of a finite membrane patch is necessary (6,29), since a continuous membrane, traditionally used in MD simulations, hinders the formation of local membrane curvature. The discontinuous-membrane setup indeed permits simulation of membrane curvature as shown in Arkhipov et al. (29) and Chandler et al. (6). NaCl was added at 150 mM concentration to the system, which

**TABLE 1** Summary of simulations performed

System	Number of atoms	Potentials applied	Simulation time
Sim1-MDFF	688,373	$U_{MD}^*$ , $U_{SS}^\dagger$ , $U_{EM}^\dagger$	5 ns
Sim1-eq-1	688,373	$U_{MD}^*$ , $U_{SS}^\dagger$	10 ns
Sim1-eq-2	688,373	$U_{MD}^*$	19 ns
Sim2-MDFF	890,307	$U_{MD}^*$ , $U_{SS}^\dagger$ , $U_{EM}^\dagger$	17 ns

\*Applied to all atoms in the system.

†Applied only to atoms of the RC-LH1-PufX dimer.

altogether contained 688,373 atoms. Snapshots of the initial system are shown in Fig. 2 A.

Simulation Sim2 used the same protein-membrane setup, but the water box was extended in the direction perpendicular to the membrane plane to ensure even better than in case of simulation Sim1 that the membrane curvature observed is not restricted by the size of the water box. The water box in Sim2 measures  $350 \text{ \AA} \times 200 \text{ \AA} \times 140 \text{ \AA}$ . After adding 150 mM NaCl, Sim2 contained 890,307 atoms. As shown in Results, the membrane patches in Sim1 and Sim2 both attained a similar degree of curvature, demonstrating that the water box in Sim1 is actually sufficiently large.

## The MDFF method

The MDFF method permits us to flexibly fit a biomolecule into an EM map within the framework of a typical MD simulation, preserving the correct

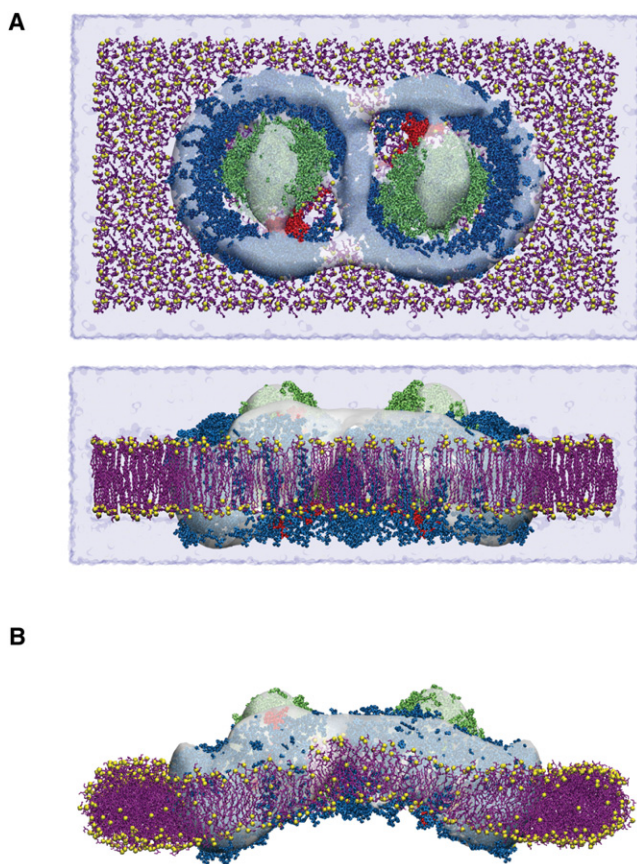


**FIGURE 2** (A) Setup of the MDFF simulation (Sim1, Table 1), shown in top and side views. The water box is rendered in transparent blue, lipid in purple with the phosphorus atoms drawn as yellow spheres, LH1 in blue, RC in green, and PufX in red. The EM map from Qian et al. (15) is shown as a transparent surface. (B) Snapshot of the system after 5 ns of MDFF simulation from Sim1; water is omitted for clarity.

stereochemistry of the molecule while accounting for the EM data (21). In MDFF, two external potentials ( $U_{EM}$ ,  $U_{SS}$ ) are added to the usual MD potential ( $U_{MD}$ ):

$$U_{\text{total}} = U_{MD} + U_{EM} + U_{SS}. \quad (1)$$

In Eq. 1, the external potential  $U_{EM}$ , derived from the EM map, steers the atoms into high-density areas;  $U_{SS}$  imposes harmonic restraints to preserve secondary structure and prevent overfitting, a common concern in flexible fitting methods (21).

A rigid-body docking was first performed in vacuo to place the dimer model into the EM density map of the *Rba. sphaeroides* RC-LH1-PufX dimer using the Situs package (30). The MDFF simulation was then performed using NAMD (31), with the external potentials applied using grid-steered molecular dynamics (32). For the MD potential ( $U_{MD}$  in Eq. 1), the CHARMM27 force field (33,34) with the CMAP correction (35) was chosen. Water molecules were described with the TIP3P model (36). Long-range electrostatic forces were evaluated through the particle-mesh Ewald summation method with a grid size of  $< 1 \text{ \AA}$ . An integration time step of 1 fs was used in the framework of a multiple time-stepping algorithm (37,38). Bonded terms were evaluated every time step, with short-range nonbonded terms evaluated every second time step and long-range electrostatics every fourth time step. Constant temperature ( $T = 300 \text{ K}$ ) was maintained using Langevin dynamics (39), with a damping coefficient of  $1.0 \text{ ps}^{-1}$ . A constant pressure of 1 atm was enforced using a Nosé-Hoover Langevin piston with a decay period of 100 fs and time constant 50 fs. The methodology is reviewed in Phillips et al. (31).

Only dimer atoms were coupled to the additional MDFF potentials  $U_{EM}$  and  $U_{SS}$ ; the rest of the system, i.e., lipid, water, and ions, was subjected only to  $U_{MD}$  and, thereby, was free to equilibrate. The MDFF potentials  $U_{EM}$  and  $U_{SS}$  contain adjustable parameters as described in Trabuco et al. (21). For our study,  $\xi = 0.3 \text{ kcal mol}^{-1}$  and  $k_{\mu} = 200 \text{ kcal mol}^{-1} \text{ \AA}^{-2}$  were used.

In Sim1, to obtain a physiologically realistic protein-membrane system, 29 ns of equilibration was performed following the 5-ns MDFF simulation (Table 1). In Sim2, MDFF was applied for the entire 17 ns of the simulation.

## Membrane curvature analysis

Measurement of membrane curvature properties requires a quantitative description of the membrane's shape. Hence, a shape-fitting protocol (Fig. S2) was developed to capture the curved surface of the membrane. The  $320 \text{ \AA} \times 170 \text{ \AA}$  lipid patch was first divided into  $5 \text{ \AA} \times 5 \text{ \AA}$  vertical square prisms parallel to the  $z$  axis (Fig. S2 A). The positions of the lipid heavy atoms within each square prism were averaged (Fig. S2 A-iii), giving an approximate shape of the membrane (Fig. S2 B). A best-fit surface was then computed for the averaged membrane shape through least-squares fitting (Fig. S2 C). The mathematical expression for the best-fit surface is user-defined; for the membrane patches in Sim1 and Sim2, because of their simple geometry, a three-dimensional quadratic equation describes their curvature sufficiently well. This equation has the general form

$$z(x, y) = a + bx + cx^2 + dy + exy + fy^2. \quad (2)$$

For a complex membrane shape with many bends and curves, a higher-order equation would be needed for the fitting. The  $z$  axis in Eq. 2 is chosen to be the direction perpendicular to the flat membrane plane at time  $t = 0$ , and the  $x$  and  $y$  axes are defined in Fig. S2 A, with the  $x$  axis being the long axis of the dimer and the  $y$  axis being the short axis. Coefficients  $a$ ,  $b$ ,  $c$ ,  $d$ ,  $e$ , and  $f$  are free parameters determined during the fitting.

Once a best-fit surface in the form of Eq. 2 is obtained, radii of curvature can be computed both along the  $x$  axis ( $r_x$ ) and the  $y$  axis ( $r_y$ ) for each point  $P = (x, y)$  (Fig. S2 D). The radius of curvature along the  $x$  axis at point  $P$  is computed by measuring the radius of the osculating circle (the circle that has the same curvature as  $P$ ), passing point  $P$  that lies in the  $x$ - $z$  plane. The radius

of curvature along the  $y$  axis,  $r_y$ , is defined similarly. Given a surface defined by Eq. 2,  $r_x$  and  $r_y$  can be readily evaluated via the general expressions (40)

$$r_x = \frac{[1 + (\frac{dz}{dx}|_y})^2]^{3/2}}{\frac{d^2z}{dx^2}|_y} = \frac{[1 + (b + ey + 2cx)^2]^{3/2}}{2c}, \quad (3)$$

and

$$r_y = \frac{[1 + (\frac{dz}{dy}|_x})^2]^{3/2}}{\frac{d^2z}{dy^2}|_x} = \frac{[1 + (d + ex + 2fy)^2]^{3/2}}{2f}. \quad (4)$$

The curvature at point  $P$ ,  $\kappa_x$  and  $\kappa_y$ , is then given by  $\kappa_x = 1/r_x$  and  $\kappa_y = 1/r_y$ .

## RESULTS

The *Rba. sphaeroides* RC-LH1-PufX dimer is known to form, in LH2-deficient mutants, tubular membrane vesicles with radii in the range of 250–550 Å (8,15–18), suggesting that the dimeric protein induces anisotropic membrane curvature. Here, we present the curvature effects of the *Rba. sphaeroides* RC-LH1-PufX dimer observed in simulations using MDFF.

### Molecular dynamics flexible fitting of the RC-LH1-PufX dimer

So far, MDFF simulations, for the sake of computational efficiency, were performed in vacuo (21,22). However, in the case of the *Rba. sphaeroides* RC-LH1-PufX dimer, lipid molecules, as well as water and ions, were included in the simulation. Only atoms belonging to the RC-LH1-PufX dimer were coupled to the MDFF potentials ( $U_{EM}$  and  $U_{SS}$  in Eq. 1); lipids, water, and ions were free to equilibrate around the protein. All atoms in the system were also subject to the MD potential ( $U_{MD}$  in Eq. 1). Such setup allowed the membrane to realistically respond to the protein's change of shape under physiological conditions.

With the MDFF settings chosen as described in Methods, the RC-LH1-PufX dimer was fitted into the EM map within a few nanoseconds. The local cross-correlation coefficient, which measures the quality of the fit, improved from 0.37 (value after rigid-body docking) to 0.65 for the 5-ns MDFF in Sim1, and from 0.37 to 0.69 in Sim2 (with a threshold of  $0.1\sigma$  above the mean (21)). The initially flat dimer, after the 5 ns of fitting in Sim1, was highly bent in accordance with the EM map geometry. Nearby lipids followed the dimer's bending and quickly developed a high local curvature. However, lipids farther away from the dimer remained flat, presumably because of insufficient time for proper equilibration (Fig. 2 B).

To give lipids the opportunity to relax, as well as to obtain a relaxed RC-LH1-PufX structure, the MDFF forces were gradually turned off. To ensure that the protein equilibrated properly, a two-step equilibration protocol followed: in the first 10 ns after the MDFF simulation, the external fitting

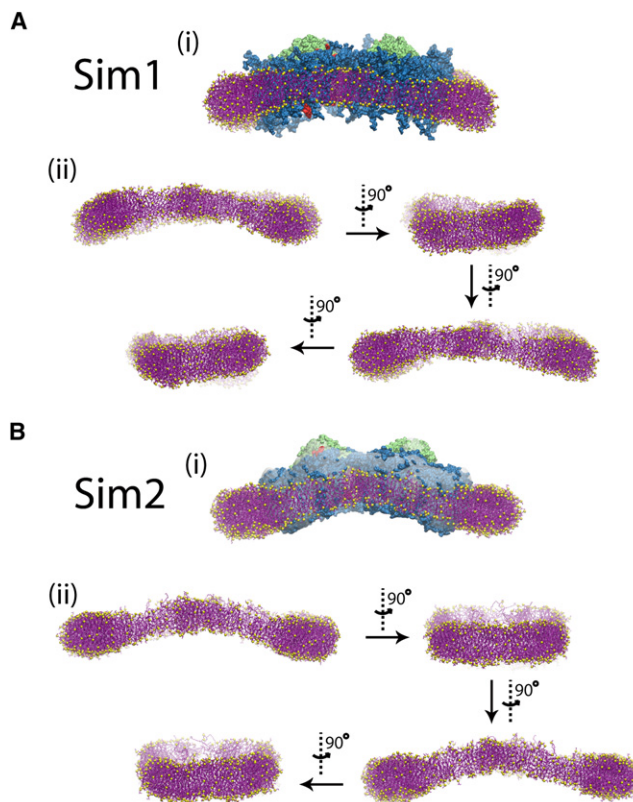


FIGURE 3 Protein-lipid system at the end of (A) Sim1 and (B) Sim2. The coloring scheme is the same as in Fig. 2. In (A-ii) and (B-ii), the RC-LH1-PufX dimer is not shown to better display the membrane geometry.

potential was turned off, but the secondary structure restraints remained on ( $U_{EM}$  off and  $U_{SS}$  on), followed by another 19 ns without secondary structure restraints ( $U_{EM}$  off and  $U_{SS}$  off; see also Table 1). After the full 29-ns equilibration, lipids farther away from the protein curved downward and the entire lipid patch became arched (Fig. 3 A-i). When viewed along the long dimer axis, the simulated membrane patch does not exhibit curvature, illustrating the anisotropy of RC-LH1-PufX dimer's curvature effect (Fig. 3 A-ii). A 360° view shows that the arched membrane patch is not completely symmetric; in addition to bending, the membrane patch also appears twisted around the long dimer axis (Fig. 3 A-ii). An animated trajectory of Sim1 is provided in Movie S1 in the Supporting Material.

In a second MDFF simulation, Sim2 (Table 1, Fig. 3 B), the MDFF forces remained on throughout the entire simulation. The resulting membrane patch is shown in Fig. 3 B. The membrane in the extended fitting simulation also curved and formed an arch similar to the one seen in Sim1. Rotating the view of the membrane patch shows that the curvature of the membrane is again anisotropic (Fig. 3 B-ii). However, the membrane patch is nearly symmetric, unlike in the case of Sim1 when the asymmetry developed in the free MD simulation after MDFF forces were turned off. An animated trajectory of Sim2 is provided in Movie S2.

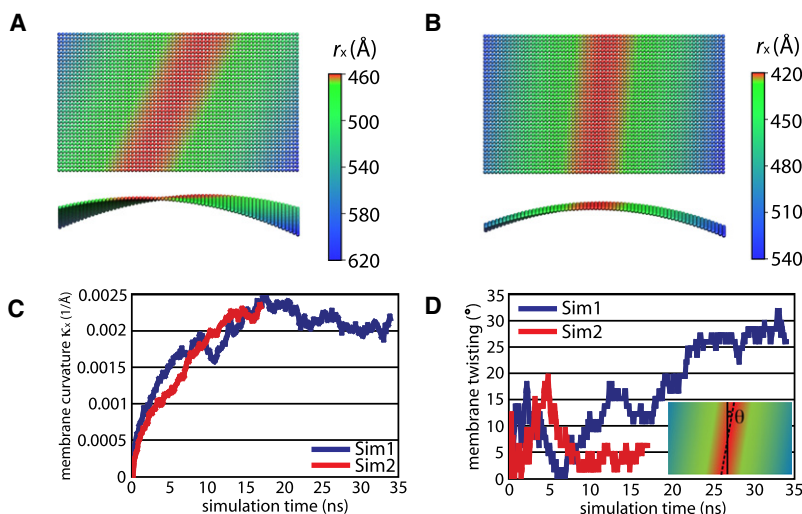


FIGURE 4 Analysis of membrane curvature shaped by the RC-LH1-PufX dimer in Sim1 and Sim2. (A) Best-fit surface for the membrane patch at the end of Sim1. The surface is colored by  $r_x$  at each point. Maximum curvature is colored red, representing  $r_x = 460$  Å. (B) Best-fit surface for the membrane patch in Sim2. Maximum curvature corresponds to  $r_x = 420$  Å. The membrane surface resulting in Sim2 is visibly less twisted than that in Sim1, as reflected in a smaller slant of the curvature pattern. (C) Measurement of membrane curvature ( $\kappa_x = 1/r_x$ ) over simulation time. The membrane patch in Sim2 attained a similar degree of curvature as seen in Sim1. (D) Measurement of membrane twisting over simulation time. Although the membrane patch generated in Sim1 shows significant membrane twisting ( $\theta_{\text{Sim1}} \sim 30^\circ$ ), the membrane patch generated in Sim2 shows less twisting ( $\theta_{\text{Sim2}} \sim 5^\circ$ ).

### Local curvature properties of RC-LH1-PufX dimer

Curvature of the membrane patches from Sim1 and Sim2 was analyzed as described in Methods, and radii of curvature,  $r_x$  and  $r_y$ , were computed using Eqs. 3 and 4. For the membrane patch in Sim1, the radius of curvature along the  $x$  axis was measured to be 460–620 Å at the end of the simulation (see Fig. 4 A), where 460 Å reflects the maximum curvature produced by the dimer, within the range of the known radius of an RC-LH1-PufX tubular vesicle at 250–550 Å (8,15–18). The twist in the membrane's curvature becomes evident through a slant in the pattern in Fig. 4 A, the pattern generated by coloring the best-fit surface according to its curvature at each point. The curvature along the  $y$  axis is significantly smaller ( $r_y = 7490$ – $8000$  Å) than the curvature along the  $x$  axis, confirming quantitatively that the curvature produced by the RC-LH1-PufX dimer is anisotropic.

The curvature properties of the membrane patch in Sim2 are much like those of Sim1 in terms of maximum curvature achieved ( $r_x \sim 420$  Å, Fig. 4 B) and anisotropy. However, the membrane is less twisted, as reflected in the less pronounced slant in Fig. 4 B compared to that seen in the case of Sim1 (Fig. 4 A). Tracking curvature over simulation time, the membrane in Sim2 reached a similar degree of curvature as found in Sim1 (Fig. 4 C). To compare the asymmetry of the membrane patches, we define the twisting angle of the membrane patch,  $\theta$ , to be the angle made by the dimer short axis and the axis of maximum curvature, with  $\theta = 0$  corresponding to a completely symmetric surface (Fig. 4 D, inset). Measurement of  $\theta$  over simulation time shows that the twisting of the membrane patch in Sim1 reached  $\sim 30^\circ$ , whereas the twisting in the case of Sim2 settled at  $\sim 5^\circ$  at the end of the simulation (Fig. 4 D). Confining the RC-LH1-PufX dimer in the EM map, therefore, produced less asymmetry in the membrane curvature. The implications of this asymmetry on RC-LH1-PufX's global curvature effects are discussed in the next section.

To visualize the dynamic membrane curvature formation during Sim1 and Sim2, the membrane curvature analysis

protocol was repeated for each frame of the trajectories, producing best-fit surfaces of the membrane patches throughout the entire simulations. In Supporting Material we provide animations of the membrane curvature development in Sim1 (Movie S3) and Sim2 (Movie S4). In Movie S3, one can recognize that the asymmetry in RC-LH1-PufX's curvature effects did not become visible until after 5 ns, i.e., until after MDFP forces were gradually turned off. In Movie S4, it can be seen that the shape of the membrane remained more symmetric, i.e., untwisted, while curvature developed.

### The effect of membrane patch twisting on the organization of *Rba. sphaeroides* tubes

The twisting of the membrane patch around the RC-LH1-PufX dimer, characterized by the twisting angle  $\theta$  as defined in Fig. 4 D, has direct implications for how the dimers are arranged in the tubular vesicles in LH2-deficient *Rba. sphaeroides*. To demonstrate the relationship between dimer-induced membrane twisting and the packing arrangement of the dimers, we use as an example the RC-LH1-PufX dimer resulting from Sim1, since Sim1 exhibits a much larger twisting angle than the case of Sim2. As shown in Fig. 5 A, if the RC-LH1-PufX dimers resulting from Sim1 are stacked directly along their short dimer axes, their local curvatures are not complementary and, therefore, they do not produce a regular tubular surface. However, if the RC-LH1-PufX dimers are placed with an offset that aligns each dimer's axis of maximum curvature, then the dimers' local curvatures become complementary and a tubular surface results (Fig. 5 B). Therefore, the twisting of the RC-LH1-PufX dimer's curvature translates to a stacking offset between two dimers.

The packing arrangement of RC-LH1-PufX was further explored by constructing two all-atom tubular vesicles, one built with the RC-LH1-PufX dimers stacked along their short dimer axes (Fig. 5 C-i), and the other built by stacking the dimers with a slight offset (Fig. 5 C-ii). Compared to the

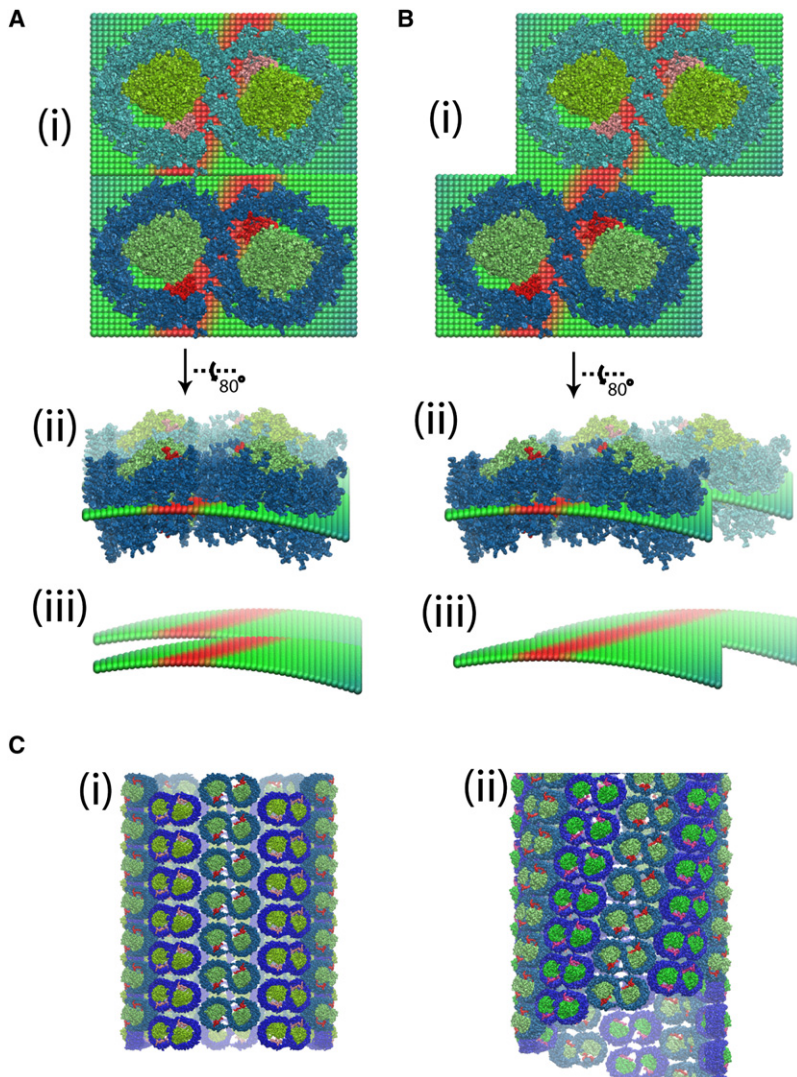


FIGURE 5 Local curvature properties of the RC-LH1-PufX dimer and the long-range organization of native *Rba. sphaeroides* tubes. (A) In a stacking arrangement in which LH1-RC-PufX dimers are placed directly on top of each other, their local curvatures cannot complement each other. (B) In a stacking arrangement in which dimers are placed with a slight offset that aligns their maximum curvature axes, their local curvature effects are complementary and form a cylindrical surface. (C) Two LH1-RC-PufX tubular vesicles were constructed—one with the lined-up stacking arrangement, and one with the offset stacking arrangement. The second arrangement (C-ii) better resembles the recent EM image of the native RC-LH1-PufX tubular vesicle (15).

EM image of a native RC-LH1-PufX tube from LH2-deficient *Rba. sphaeroides*, which shows that the dimers are organized in a helical arrangement (15), the tubular vesicle in Fig. 5 C-ii matches the EM image better. Therefore, the offset stacking arrangement of RC-LH1-PufX dimers that leads to the helical organization of the dimers, i.e., a global effect, can be explained by the twisting of the RC-LH1-PufX dimer's local curvature.

### Correlation of relative RC orientation and membrane shape

To investigate how membrane twisting, which is more pronounced in Sim1 than in Sim2, is related to the internal structure of the RC-LH1-PufX dimer, structural changes of the dimer over the course of the simulations were monitored (Fig. S3). Sim1 and Sim2 started with the same protein-lipid system that was symmetric by construction, with the RCs sitting upright with respect to the membrane plane. By the end of Sim1, the two LH1 monomers swung in opposite

directions: as shown in Fig. S3 A-ii, the RC-LH1-PufX monomer closer to the view rotated around the long dimer axis in the counterclockwise direction, while the other monomer rotated in the opposite direction, faintly seen in the background. Within the LH1 monomers, the RCs have similarly tilted away from their initial upright position (Fig. S3 B-ii). Unlike in Sim1, the RCs in Sim2 stayed approximately vertical (Fig. S3 B-iii) as the surrounding LH1 helices remained upright (Fig. S3 C-iii). The two RC-LH1-PufX monomers did not tilt, and the membrane remained more symmetric than seen in Sim1. Therefore, despite the RCs being situated deep inside the RC-LH1-PufX complex and not interacting with the curved membrane directly, through hydrophobic interactions with the LH1 the relative orientation of the two RCs is seen to be correlated with both the geometry of the dimer and, consequently, with the dimer's membrane curvature properties.

This observation is consistent with our previous simulations (6) and earlier findings indicating that whereas dimeric RC-LH1-PufX complexes are located in curved membranes,

monomeric RC-LH1 rings in *Rba. sphaeroides* mutants lacking PufX and LH2 occupy flat membranes (41,42). Within an RC-LH1-PufX dimer, the two RCs have a particular orientation within their respective LH1 ring (10,43), thereby confining the two RCs to a specific relative position forming a curved hydrophobic region when viewed along the membrane plane that matches the bent shape of the surrounding LH1, which causes the membrane to bend (6). For the RC-LH1 monomers, there is no pairwise restriction to RC orientations; i.e., in an array of RC-LH1 monomers, the RCs exhibit no ordered relative orientations (43), while global curvature is not seen in the membrane.

### Structural features of the bent RC-LH1-PufX dimer model

The MDFF simulation, followed by a 29-ns equilibration in Sim1, provided an atomic model for the bent RC-LH1-PufX dimer. A discussion on the structural aspects of the resulting RC-LH1-PufX protein model is presented in [Supporting Material](#); the pigment organization within the RC-LH1-PufX dimer that resulted from the MDFF simulations is discussed in Şener et al. (23).

## DISCUSSION

Membrane proteins, such as the *Rba. sphaeroides* RC-LH1-PufX dimer, have long been suggested to shape their membrane environment (1–5,44). Through experimental methods (e.g., mutation studies and in vitro protein/lipid reconstitution), a few integral membrane proteins have been found to induce the formation of large-scale membrane structures, examples including the reticulon protein family, the DP1/Yop1p proteins, and the bacterial light-harvesting proteins (2,16,45,46). Only recently has direct observation of the dynamic process of membrane reshaping using MD been achieved at all-atom resolution ((6,29,47–50) (D. Chandler, J. Gumbart, and K. Schulten, unpublished)), allowing the identification of membrane-shaping mechanisms otherwise difficult to probe via experimental means. All-atom MD, however, requires high-resolution protein structures, and among the few known membrane-bending proteins, even fewer have available structures. For this reason, determining protein structure through low-resolution EM data, using a combination of modeling and flexible fitting methods (21,52–61), can contribute to the understanding of not only the protein's structure, but also its membrane curvature properties.

The simulations performed in this study represent a successful example of extracting atomistic information from a low-resolution EM map. A low-resolution density map of the bent, dimeric *Rba. sphaeroides* RC-LH1-PufX was combined with a modeled all-atom structure using the MDFF method (21) to reproduce and characterize the protein's membrane curvature effects, otherwise difficult given the lack of high-resolution data. The local curvature effects observed also offer

an understanding of the global curvature produced by aggregates of the protein. Although the *Rba. sphaeroides* RC-LH1-PufX dimer structure still needs to become better resolved to address issues such as the location of PufX and the mechanism of RC-LH1-PufX dimerization, curvature properties of RC-LH1-PufX can already be preliminarily described, given that the dimer's membrane-bending characteristics arise mainly from the interactions between lipids and the transmembrane LH1 helices, which are arranged in a distinct V-shape readily identified in the low-resolution EM map (15). In other words, MDFF could identify the correct placements of LH1 transmembrane helices at the edge of the RC-LH1-PufX dimer even if it might not yet attribute their placements to the exact causes, e.g., to a yet to be determined molecular role of PufX. Indeed, earlier simulations performed in Chandler et al. (6) showed that excluding PufX (by replacing the PufX helices with lipids) in the RC-LH1-PufX protein-lipid system resulted in a degree of membrane curvature similar to the system with PufX in the few tens of nanoseconds of MD equilibration. Therefore, PufX, which is suggested to be situated within the RC-LH1-PufX dimer in both arrangements proposed thus far (7–13), should not affect the membrane curvature observed here through MDFF simulations. Although the absence of PufX in vivo does abolish the curvature of the photosynthetic membrane as the RC-LH1 complexes form monomers instead of bent dimers (8), the molecular effect of PufX on RC-LH1-PufX curvature properties may not have been seen in the earlier (6) or present simulations, perhaps because of the longer timescale required for such effect to take place.

It is still not completely understood why some cellular proteins evolved to actively produce membrane curvature. In the case of the RC-LH1-PufX dimer, it has been suggested that vesiculation of the membrane increases the light-absorption area (15,62). However, there are also bacterial species with flat photosynthetic membranes and these species are as viable as those with curved photosynthetic membranes (63–65). Another reason for the RC-LH1-PufX dimer to curve the membrane might be to drive the formation of photosynthetic domains in which the photosynthetic proteins are tightly packed. Previous Monte Carlo simulations demonstrated that membrane proteins with similar shape and curvature properties attract and aggregate in the membrane, leading to the formation of high-curvature regions where the proteins crowd tightly (43,66). Such curvature-driven aggregation of integral membrane proteins was also observed experimentally for rhodopsin (67). Being in close proximity is essential for the efficient energy transfer between light-harvesting proteins since energy transfer is more rapid when protein-protein distances are shorter (23,68). It is possible, therefore, that the RC-LH1-PufX dimers utilize their curvature property to attract each other in the membrane, facilitating their light-harvesting function.

In total, we have demonstrated that a large degree of bending in a dimeric integral membrane protein can induce

high local curvature in its surrounding lipid environment. With this knowledge, simplified (i.e., coarser) descriptions with appropriately assigned local curvature properties can be developed to investigate large-scale membrane reshaping and tubulation induced by a collection of RC-LH1-PufX dimers. It is also possible to design artificial proteins with specific geometric features to create localized membrane geometries of choice, and even artificially produce membrane vesicles and tubular structures.

## SUPPORTING MATERIAL

Five figures, one table, four movies, and additional results are available at [http://www.biophysj.org/biophysj/supplemental/S0006-3495\(09\)00856-X](http://www.biophysj.org/biophysj/supplemental/S0006-3495(09)00856-X).

The authors thank Melih Şener for helpful discussions and readings of the manuscript, as well as D. E. Chandler, C. B. Harrison, and P. L. Freddolino for much assistance. Molecular images in this article were generated with the molecular graphics program VMD (69).

This work was supported by National Science Foundation grant No. MCB0744057 and National Institutes of Health grant No. P41-RR005969. Computer time was provided by the National Center for Supercomputing Applications and the Texas Advanced Computing Center via Large Resources Allocation Committee grant No. MCA93S028, and resources of the Argonne Leadership Computing Facility at Argonne National Laboratory, which is supported by the Office of Science of the U.S. Department of Energy under contract No. DE-AC02-06CH11357.

## REFERENCES

- Dudkina, N. V., J. Heinemeyer, W. Keegstra, E. J. Boekema, and H.-P. Braun. 2005. Structure of dimeric ATP synthase from mitochondria: an angular association of monomers induces the strong curvature of the inner membrane. *FEBS Lett.* 579:5769–5772.
- McMahon, H. T., and J. L. Gallop. 2005. Membrane curvature and mechanisms of dynamic cell membrane remodeling. *Nature.* 438:590–596.
- Zimmerberg, J., and M. M. Kozlov. 2006. How proteins produce cellular membrane curvature. *Nat. Rev. Mol. Cell Biol.* 7:9–19.
- Collins, R. N. 2006. How the ER stays in shape. *Cell.* 124:464–466.
- Strauss, M., G. Hofhaus, R. R. Schröder, and W. Kühlbrandt. 2008. Dimer ribbons of ATP synthase shape the inner mitochondrial membrane. *EMBO J.* 27:1154–1160.
- Chandler, D., J. Hsin, C. B. Harrison, J. Gumbart, and K. Schulten. 2008. Intrinsic curvature properties of photosynthetic proteins in chromatophores. *Biophys. J.* 95:2822–2836.
- Scheuring, S., F. Francia, J. Busselez, B. A. Melandris, J.-L. Rigaud, et al. 2004. Structural role of PufX in the dimerization of the photosynthetic core complex of *Rhodobacter sphaeroides*. *J. Biol. Chem.* 279:3620–3626.
- Siebert, C. A., P. Qian, D. Fotiadis, A. Engel, C. N. Hunter, et al. 2004. Molecular architecture of photosynthetic membranes in *Rhodobacter sphaeroides*: the role of PufX. *EMBO J.* 23:690–700.
- Scheuring, S., J. Busselez, and D. Lévy. 2005. Structure of the dimeric PufX-containing core complex of *Rhodobacter blasticus* by *in situ* atomic force microscopy. *J. Biol. Chem.* 280:1426–1431.
- Qian, P., C. N. Hunter, and P. A. Bullough. 2005. The 8.5 Å projection structure of the core RC-LH1-PufX dimer of *Rhodobacter sphaeroides*. *J. Mol. Biol.* 349:948–960.
- Cogdell, R. J., A. Gall, and J. Köhler. 2006. The architecture and function of the light-harvesting apparatus of purple bacteria: from single molecules to *in vivo* membranes. *Q. Rev. Biophys.* 39:227–324.
- Scheuring, S. 2006. AFM studies of the supramolecular assembly of bacterial photosynthetic core-complexes. *Curr. Opin. Struct. Biol.* 10:1–7.
- Busselez, J., M. Cottevielle, P. Cuniassé, F. Gubellini, N. Boisset, et al. 2007. Structural basis for the PufX-mediated dimerization of bacterial photosynthetic core complexes. *Structure.* 15:1674–1683.
- Holden-Dye, K., L. I. Crouch, and M. R. Jones. 2008. Structure, function and interactions of the PufX protein. *Biochim. Biophys. Acta.* 1777:613–630.
- Qian, P., P. A. Bullough, and C. N. Hunter. 2008. Three-dimensional reconstruction of a membrane-bending complex: the RC-LH1-PufX core dimer of *Rhodobacter sphaeroides*. *J. Biol. Chem.* 283:14002–14011.
- Kiley, P. J., A. Varga, and S. Kaplan. 1988. Physiological and structural analysis of light-harvesting mutants of *Rhodobacter sphaeroides*. *J. Bacteriol.* 170:1103–1115.
- Hunter, C. N., J. D. Pennoyer, J. N. Sturgis, D. Farrelly, and R. A. Niederman. 1988. Oligomerization states and associations of light-harvesting pigment protein complexes of *Rhodobacter sphaeroides* as analyzed by lithium dodecyl sulfate-polyacrylamide gel electrophoresis. *Biochemistry.* 27:3459–3467.
- Jungas, C., J. Ranck, J. Rigaud, P. Joliot, and A. Verméglio. 1999. Supramolecular organization of the photosynthetic apparatus of *Rhodobacter sphaeroides*. *EMBO J.* 18:534–542.
- Westerhuis, W. H. J., J. N. Sturgis, E. C. Ratcliffe, C. N. Hunter, and R. A. Niederman. 2002. Isolation, size estimates, and spectral heterogeneity of an oligomeric series of light-harvesting 1 complexes from *Rhodobacter sphaeroides*. *Biochemistry.* 41:8698–8707.
- Oelze, J., and G. Drews. 1972. Membranes of photosynthetic bacteria. *Biochim. Biophys. Acta.* 265:209–239.
- Trabuco, L. G., E. Villa, K. Mitra, J. Frank, and K. Schulten. 2008. Flexible fitting of atomic structures into electron microscopy maps using molecular dynamics. *Structure.* 16:673–683.
- Villa, E., J. Sengupta, L. G. Trabuco, J. LeBarron, W. T. Baxter, et al. 2009. Ribosome-induced changes in elongation factor Tu conformation control GTP hydrolysis. *Proc. Natl. Acad. Sci. USA.* 106:1063–1068.
- Şener, M. K., J. Hsin, L. G. Trabuco, E. Villa, P. Qian, et al. 2009. Structural model and excitonic properties of the dimeric RC-LH1-PufX complex from *Rhodobacter sphaeroides*. *Chem. Phys.* 357:188–197.
- Conroy, M. J., W. Westerhuis, P. S. Parkes-Loach, P. A. Loach, C. N. Hunter, et al. 2000. The solution structure of the *Rhodobacter sphaeroides* LH1  $\beta$  reveals two helical domains separated by a more flexible region: structural consequences for the LH1 complex. *J. Mol. Biol.* 298:83–94.
- Wang, Z. Y., K. Gokan, M. Kobayashi, and T. Nozawa. 2005. Solution structures of the core light-harvesting  $\alpha$  and  $\beta$  polypeptides from *Rhodospirillum rubrum*: implications for the pigment-protein and protein-protein interactions. *J. Mol. Biol.* 347:465–477.
- Koepke, J., X. Hu, C. Muenke, K. Schulten, and H. Michel. 1996. The crystal structure of the light harvesting complex II (B800–850) from *Rhodospirillum rubrum*. *Structure.* 4:581–597.
- Ermiler, U., G. Fritzsche, S. K. Buchanan, and H. Michel. 1994. Structure of the photosynthetic reaction center from *Rhodobacter sphaeroides* at 2.65 Å resolution: cofactors and protein-cofactor interactions. *Structure.* 2:925–936.
- Tunncliffe, R. B., E. C. Ratcliffe, C. N. Hunter, and M. P. Williamson. 2006. The solution structure of the PufX polypeptide from *Rhodobacter sphaeroides*. *FEBS Lett.* 580:6967–6971.
- Arkhipov, A., Y. Yin, and K. Schulten. 2008. Four-scale description of membrane sculpting by BAR domains. *Biophys. J.* 95:2806–2821.
- Wriggers, W., and K. Schulten. 1999. Investigating a back door mechanism of actin phosphate release by steered molecular dynamics. *Proteins Struct. Funct. Gen.* 35:262–273.
- Phillips, J. C., R. Braun, W. Wang, J. Gumbart, E. Tajkhorshid, et al. 2005. Scalable molecular dynamics with NAMD. *J. Comput. Chem.* 26:1781–1802.

32. Wells, D., V. Abramkina, and A. Aksimentiev. 2007. Exploring transmembrane transport through  $\alpha$ -hemolysin with grid-steered molecular dynamics. *J. Chem. Phys.* 127:125101–125110.
33. MacKerell, Jr., A., D. Bashford, M. Bellott, R. L. Dunbrack, Jr., J. Evans, et al. 1998. All-atom empirical potential for molecular modeling and dynamics studies of proteins. *J. Phys. Chem. B.* 102:3586–3616.
34. Foloppe, N., and A. D. MacKerell, Jr. 2000. All-atom empirical force field for nucleic acids: I. Parameter optimization based on small molecule and condensed phase macromolecular target data. *J. Comput. Chem.* 21:86–104.
35. MacKerell, Jr., A. D., M. Feig, and C. L. Brooks III. 2004. Extending the treatment of backbone energetics in protein force fields: limitations of gas-phase quantum mechanics in reproducing protein conformational distributions in molecular dynamics simulations. *J. Comput. Chem.* 25:1400–1415.
36. Jorgensen, W. L., J. Chandrasekhar, J. D. Madura, R. W. Impey, and M. L. Klein. 1983. Comparison of simple potential functions for simulating liquid water. *J. Chem. Phys.* 79:926–935.
37. Schlick, T., R. Skeel, A. Brünger, L. Kalé, J. A. Board, Jr., et al. 1999. Algorithmic challenges in computational molecular biophysics. *J. Comput. Phys.* 151:9–48.
38. Grubmüller, H., H. Heller, A. Windemuth, and K. Schulten. 1991. Generalized Verlet algorithm for efficient molecular dynamics simulations with long-range interactions. *Mol. Simul.* 6:121–142.
39. Brünger, A. T., C. L. Brooks III, and M. Karplus. 1984. Stochastic boundary conditions for molecular dynamics simulations of ST2 water. *Chem. Phys. Lett.* 105:495–498.
40. Hyde, S., S. Andersson, K. Larsson, Z. Blum, T. Landh, et al. 1997. *The Language of Shape*. Elsevier Science, Amsterdam, The Netherlands.
41. Frese, R., J. Olsen, R. Branvall, W. Westerhuis, C. Hunter, et al. 2000. The long-range supraorganization of the bacterial photosynthetic unit: a key role for PufX. *Proc. Natl. Acad. Sci. USA.* 97:5197–5202.
42. Frese, R. N., C. A. Siebert, R. A. Niederman, C. N. Hunter, C. Otto, et al. 2004. The long-range organization of a native photosynthetic membrane. *Proc. Natl. Acad. Sci. USA.* 101:17994–17999.
43. Frese, R. N., J. C. Pàmies, J. D. Olsen, S. Bahatyrova, C. D. van der Weij-de Wit, et al. 2008. Protein shape and crowding drive domain formation and curvature in biological membranes. *Biophys. J.* 94:640–647.
44. MacKinnon, R. 2004. Voltage sensor meets lipid membrane. *Science.* 306:1304–1305.
45. Voeltz, G. K., W. A. Prinz, Y. Shibata, J. M. Rist, and T. A. Rapoport. 2006. A class of membrane proteins shaping the tubular endoplasmic reticulum. *Cell.* 124:573–586.
46. Hu, J., Y. Shibata, C. Voss, T. Shemesh, Z. Li, et al. 2008. Membrane proteins of the endoplasmic reticulum induce high-curvature tubules. *Science.* 319:1247–1250.
47. Blood, P. D., and G. A. Voth. 2006. Direct observation of Bin/amphiphysin/Rvs (BAR) domain-induced membrane curvature by means of molecular dynamics simulations. *Proc. Natl. Acad. Sci. USA.* 103:15068–15072.
48. Ayton, G. S., P. D. Blood, and G. A. Voth. 2007. Membrane remodeling from N-BAR domain interactions: insights from multi-scale simulation. *Biophys. J.* 92:3595–3602.
49. Blood, P. D., R. D. Swenson, and G. A. Voth. 2008. Factors influencing local membrane curvature induction by N-BAR domains as revealed by molecular dynamics simulations. *Biophys. J.* 95:1866–1876.
50. Marrink, S. J., A. H. de Vries, and D. P. Tieleman. 2008. Lipids on the moves: simulations of membrane pores, domains, stalks and curves. *Biochim. Biophys. Acta.* 1788:149–168.
51. Reference deleted in proof.
52. Jolley, C. C., S. A. Wells, P. Fromme, and M. F. Thorpe. 2008. Fitting low-resolution cryo-EM maps of proteins using constrained geometric simulations. *Biophys. J.* 94:1613–1621.
53. Topf, M., K. Lasker, B. Webb, H. Wolfson, W. Chiu, et al. 2008. Protein structure fitting and refinement guided by cryo-EM density. *Structure.* 16:295–307.
54. Chapman, M. S. 1995. Restrained real-space macromolecular atomic refinement using a new resolution-dependent electron-density function. *Acta Crystallogr. A.* 51:69–80.
55. Chen, L. F., E. Blanc, M. S. Chapman, and K. A. Taylor. 2001. Real space refinement of acto-myosin structures from sectioned muscle. *J. Struct. Biol.* 133:221–232.
56. Wriggers, W., and S. Birmanns. 2001. Using Situs for flexible and rigid-body fitting of multiresolution single-molecule data. *J. Struct. Biol.* 133:193–202.
57. Tama, F., O. Miyashita, and C. L. Brooks III. 2004. Flexible multi-scale fitting of atomic structures into low-resolution electron density maps with elastic network normal mode analysis. *J. Mol. Biol.* 337:985–999.
58. Suhre, K., J. Navaza, and Y. H. Sanejouand. 2006. NORMA: a tool for flexible fitting of high-resolution protein structures into low-resolution electron-microscopy-derived density maps. *Acta Crystallogr. D Biol. Crystallogr.* 62:1098–1100.
59. Velazquez-Muriel, J. A., M. Valle, A. Santamaría-Pang, I. A. Kakadiaris, and J. M. Carazo. 2006. Flexible fitting in 3D-EM guided by the structural variability of protein superfamilies. *Structure.* 14:1115–1126.
60. Kovacs, J. A., M. Yeager, and R. Abagyan. 2008. Damped-dynamics flexible fitting. *Biophys. J.* 95:3192–3207.
61. Orzechowski, M., and F. Tama. 2008. Flexible fitting of high-resolution x-ray structures into cryo electron microscopy maps using biased molecular dynamics simulations. *Biophys. J.* 95:5692–5705.
62. Şener, M. K., J. D. Olsen, C. N. Hunter, and K. Schulten. 2007. Atomic level structural and functional model of a bacterial photosynthetic membrane vesicle. *Proc. Natl. Acad. Sci. USA.* 104:15723–15728.
63. Sturgis, J. N., and R. A. Niederman. 1996. The effect of different levels of the B800–B850 light-harvesting complex on intracytoplasmic membrane development in *Rhodobacter sphaeroides*. *Arch. Microbiol.* 165:235–242.
64. Hickman, D. D., and A. W. Frenkel. 1965. Observations on the structure of *Rhodospirillum molischianum*. *J. Cell Biol.* 25:261–278.
65. Miller, K. R. 1979. Structure of a bacterial photosynthetic membrane. *Proc. Natl. Acad. Sci. USA.* 76:6415–6419.
66. Reynwar, B. J., G. Illya, V. A. Harmandaris, M. M. Müller, K. Kremer, et al. 2007. Aggregation and vesiculation of membrane proteins by curvature-mediated interactions. *Nature.* 447:461–464.
67. Botelho, A. V., T. Huber, T. P. Sakmar, and M. F. Brown. 2006. Curvature and hydrophobic forces drive constitutive association and modulate activity of rhodopsin in membranes. *Biophys. J.* 91:4464–4477.
68. Ritz, T., S. Park, and K. Schulten. 2001. Kinetics of excitation migration and trapping in the photosynthetic unit of purple bacteria. *J. Phys. Chem. B.* 105:8259–8267.
69. Humphrey, W., A. Dalke, and K. Schulten. 1996. VMD—visual molecular dynamics. *J. Mol. Graph.* 14:33–38.